

## Three-nucleon mechanisms in photoreactions

D.P. Watts<sup>a</sup> J. Ahrens<sup>b</sup> J.R.M. Annand<sup>a</sup> R. Beck<sup>b</sup> D. Branford<sup>c</sup> P. Grabmayr<sup>d</sup> T. Hehl<sup>d</sup> J.D. Kellie<sup>a</sup>  
I.J.D. MacGregor<sup>a</sup> J.C. McGeorge<sup>a</sup> R.O.Owens<sup>a</sup>

<sup>a</sup>Department of Physics and Astronomy, University of Glasgow, Glasgow, G12 8QQ, UK.

<sup>b</sup>Institut für Kernphysik, Universität Mainz, D-55099 Mainz, Germany

<sup>c</sup>Department of Physics and Astronomy, University of Edinburgh, Edinburgh EH9 3JZ, UK

<sup>d</sup>Physikalisches Institut, Universität Tübingen, D-72076 Tübingen, Germany

The  $^{12}\text{C}(\gamma, ppn)$  reaction has been measured for  $E_\gamma=150\text{-}800$  MeV in the first study of this reaction in a target heavier than  $^3\text{He}$ . The experimental data are compared to a microscopic many body calculation. The model, which predicts that the largest contribution to the reaction arises from final state interactions following an initial pion production process, overestimates the measured cross sections and there are strong indications that the overestimate arises in this two-step process. The selection of suitable kinematic conditions strongly suppresses this two-step contribution leaving cross sections in which up to half the yield is predicted to arise from the absorption of the photon on three interacting nucleons and which agree with the model. The results indicate  $(\gamma, 3N)$  measurements on nuclei may be a valuable tool for obtaining information on the nuclear three-body interaction.

The study of  $(\gamma, 3N)$  reactions in nuclei offers a possible new means of learning about the character of three-nucleon forces (3NF), which are thought to play a small but essential role in nuclear structure and reactions[1]. Since the details of this role and the relative importance of the different 3NF mechanisms are not well established it is of interest to examine three-nucleon knockout reactions, which can take place via closely related mechanisms, to see what light they can cast on the three-nucleon force.

An early indication of the significance of the 3NF came from binding energy calculations for the few-nucleon systems, which fail to reproduce the measured binding if only the two-nucleon force is used. The present position is reviewed in [2]. The latest calculations underestimate the binding energy of  $^3\text{H}$  and  $^3\text{He}$  by  $\sim 0.5\text{-}0.9$  MeV[3,4] and of  $^4\text{He}$  by  $2.0\text{-}4.2$  MeV[3,5] but the inclusion of the 3NF largely removes these discrepancies and also reduces the disagreements observed in the description of nucleon-deuteron scattering. Residual discrepancies in the de-

scription of polarisation observables in nucleon-deuteron scattering may be attributable to additional 3NF mechanisms not presently included in the calculations.

Many 3NF models are based on  $2\pi$  exchange forces and intermediate  $\Delta$  excitation but other Feynman diagrams have been proposed, in particular short range components involving  $N^*$  excitation and the exchange of heavier mesons such as the  $\rho$  and  $\omega$ . Recent insights from chiral perturbation theory are helping to guide the development of 3NF models[1,6]. However experimental input from a range of reactions will be needed to identify the most important diagrams.

To investigate the potential of 3N knockout reactions in the study of 3NFs, it is necessary to determine the contribution made by direct 3N mechanisms to these reactions and the ease with which they can be separated from other competing mechanisms. The majority of the published work on three nucleon knockout from nuclei reports  $(\pi^+, ppp)$  measurements which have been carried out on  $^3\text{He}$ [7],  $^4\text{He}$ [7,8] and heav-

ier targets[9]. The analysis of these experiments relied on fitting the data to determine the relative strengths of the contributing reaction mechanisms, in an attempt to separate  $(\pi, 3N)$  reactions from those where the  $(\pi, 2N)$  process is preceded by  $(\pi, N)$  scattering or followed by  $(N, N')$  scattering. The fits indicate that two step processes involving initial  $(\pi, N)$  scattering contribute to the cross section at the  $\sim 25\%$  level. A strong  $(\pi, 3N)$  contribution is also suggested although significant features in the data were not accounted for. Progress towards identifying the effects of 3NFs requires a theoretical treatment which predicts at least the strength and preferably the details of the  $(\pi, 3N)$  process.

The use of photons offers advantages over pions as the weak electromagnetic interaction ensures that the full nuclear interior is sampled and that initial state interactions, which complicate pion induced reactions, are negligible. The only previous studies of  $(\gamma, 3N)$  reactions are  ${}^3\text{He}(\gamma, ppn)$ [10] and  ${}^{12}\text{C}(\gamma, ppp)$ [11] measurements. For both targets it is concluded that the main contributing mechanism is the 2-step process involving the initial production of a real pion followed by subsequent pion reabsorption ( $N\pi + ABS$ ). In [11] detailed investigation of the contribution of the 3N mechanism to the  ${}^{12}\text{C}(\gamma, ppp)$  data was not feasible due to the statistical accuracy obtained and only its contribution to two-nucleon knockout variables was studied.

With the recent advances in the experimental and theoretical study of the 3NF, it is timely to explore further what can be learnt about their nature from  $(\gamma, 3N)$  measurements on nuclei. As a first step recent data on the  ${}^{12}\text{C}(\gamma, ppn)$  reaction, obtained during a study of  ${}^{12}\text{C}(\gamma, 2N)$  processes[12], are examined. To gain sensitivity it is important to emphasize the contribution in which the photon is absorbed by three nucleons (3N).

The Valencia model (VM)[13,14] is a microscopic many-body model describing photon-nucleus interactions. Its basis is a construction of the photon self-energy in nuclear matter, which is related to the cross sections for different photon absorption mechanisms through Cutkosky rules.

A realistic matter distribution for nuclei is included in this prescription using a local density approximation. The cross sections for the absorption of the photon by two nucleons ( $2N$ ), three nucleons ( $3N$ ) and pion production processes ( $N\pi$  and  $NN\pi$ ) are obtained from this theoretical approach. The 3N mechanism includes the effects of both pion and shorter range meson exchanges but does not include resonances higher than the  $\Delta$ . Both nucleons and pions produced in the absorption process have quite large reaction cross sections in the nuclear medium and the model accounts for these final state interactions (FSI) using a semi-classical Monte Carlo simulation. The Valencia model has been shown to give a quite good general description of  $(\gamma, pn)$  reaction on  ${}^{12}\text{C}$  for  $E_\gamma = 110-500$  MeV, but overestimates the smaller  $(\gamma, pp)$  channel[11,12,16,17].

The measurements of the  ${}^{12}\text{C}(\gamma, ppn)$  cross sections reported here were made using the Glasgow photon-tagging spectrometer[18] at the Mainz 855 MeV electron microtron MAMI. The tagger produced  $\sim 10^8$  tagged photons per second in the energy range 150-800 MeV, which hit a 4mm thick graphite target. Products from the resulting photoreactions were detected in two systems - PiP[19] and TOF[20]. PiP is a large ( $\sim 1$ sr) plastic scintillator hodoscope, which was used to detect protons in the energy range  $\sim 31-290$  MeV for polar angles of  $78^\circ-153^\circ$ . The proton energy was determined from the energy deposited in the detector. TOF comprises a large plastic scintillator array which was used to detect both protons and neutrons in the energy ranges  $\sim 35-190$  MeV and  $19-640$  MeV respectively. The energies of both particle types were determined from the measured time-of-flight. TOF covered polar angles  $36^\circ-142^\circ$  opposite PiP and  $16^\circ-31^\circ$  on the PiP-side of the beam, giving a total solid angle of 0.91 sr. Reaction timing was obtained from a segmented half-ring of 1mm thick scintillators ( $\Delta E_{PiP}$ ) centred on the target and positioned on the PiP-side of the beam at a radius of  $\sim 11$  cm. Separation of uncharged and charged particles in TOF was carried out using information from  $\Delta E_{PiP}$  as well as two further half rings of 2mm thick scintillator  $\Delta E_{TOF}$  covering the TOF-side of the photon beam at radii of  $\sim 11$  cm and  $\sim 30$  cm. To re-

move ambiguities in this procedure, the two TOF particles were required to have an opening angle  $\geq 60^\circ$ . The particle selection and energy calibration methods employed in the analysis are described elsewhere[12]. The setup allows a wide kinematic coverage for emitted particles with energy resolution of  $\sim 6$  MeV (FWHM).

The effect of random coincidences in the tagger and neutron detection in TOF were accounted for using a weight method[21]. The effect of randoms for charged particle detection in PiP and TOF was negligible due to the requirement of multiple coincidences between the thick detectors and the  $\Delta E$  detectors near to the target. The sources of systematic error in the measured cross sections are discussed in ref.[11] and are estimated to be  $\pm 12\%$ . An overall check of the reliability of the measured cross sections was provided by a measurement of the  $D(\gamma, np)$ ,  $^{12}\text{C}(\gamma, np)$  and  $^{12}\text{C}(\gamma, pp)$  cross sections, which were all found to agree[12] with previous measurements[22,23] within the quoted uncertainties.

Fig. 1 shows the measured  $^{12}\text{C}(\gamma, ppn)$  cross section as a function of the three-body missing energy, defined as  $E_m^{3B} = E_\gamma - T_r - \sum_{i=1}^3 T_i$ , where  $E_\gamma$  is the incident photon energy,  $T_i$  are the kinetic energies of the three detected nucleons and  $T_r$  is the (typically small) energy of the recoiling system which is calculated from its momentum,  $\mathbf{P}_r = \mathbf{P}_\gamma - \sum_{i=1}^3 \mathbf{P}_i$ . The missing energy is the sum of the separation energy ( $S$ ) for the reaction and the excitation energy of the (A-3) residual system ( $E_X$ ),  $E_m^{3B} = S + E_X$ .

The experimental data show strength near to  $S$  (34.0 MeV) corresponding to leaving the A-3 system near to its ground state. There is however significant cross section at higher  $E_m^{3B}$  indicating a strong role for processes which leave the A-3 system highly excited, probably through the emission of more than three nucleons. Similar features are observed in  $(\pi^+, ppp)$  reactions[9].

Fig. 1 also shows the result of a VM simulation of the  $^{12}\text{C}(\gamma, ppn)$  reaction including the response of the PiP and TOF detectors. An 8 MeV correction for average nucleon binding is made as described in [11]. The contribution arising from an initial  $N\pi$  process is presented separately for cases where the pion is reab-

sorbed ( $N\pi + ABS$ ) or when the pion is emitted ( $N\pi + EMIT$ ). Because there is strong evidence from previous experiments[12,17] and the present results that the strength of the  $N\pi + ABS$  process in  $^{12}\text{C}$  is overestimated by the VM model the predictions are presented with the strength of this process reduced by the average factor 0.3 necessary to bring the model into agreement with  $^{12}\text{C}(\gamma, p)$  data[17] for the backward proton angles sampled in the present measurement. The same factor also produces much closer agreement in comparisons[12,17] with  $^{12}\text{C}(\gamma, np)$  data at backward proton angles. Overestimation of the  $\pi$  absorption process by the VM by factors of up to  $\sim 5$  has also been seen for certain kinematic regions in comparisons with  $^{12}\text{C}(\pi^+, p)$ [14] and  $^{12}\text{C}(\pi^+, ppp)$ [15] measurements.

The predicted contributions from different mechanisms (after the reduction of the  $N\pi + ABS$  strength) are separated and shown by the (stacked) shaded histograms identified in the key in Fig 1. After the reduction the model gives a good general description of both the shape and magnitude of the measured data over a wide range of  $E_\gamma$  and missing energy. The  $3N$  process gives its largest contribution at low missing energy, but even there generally contributes less than 1/3 of the cross section. Without reduction of the  $N\pi + ABS$  process the VM prediction is seen to give a much poorer description of the experimental data and in several cases the predicted  $N\pi + ABS$  contribution alone exceeds the measured cross section.

A concerted attempt to minimise the contributions of the absorption mechanisms other than  $3N$  would employ kinematic cuts based on the predicted distributions of the nucleons produced by the different mechanisms. Such predictions are not all available at present. In their absence we have made a significant reduction in the ( $N\pi + ABS$ ) contribution based on a reconstruction of the invariant mass of the pion, which is created in the first step of the process. Neglecting Fermi motion and nucleon FSI, the invariant mass ( $M_X$ ) of the object  $X$  in an assumed  $\gamma + N \rightarrow N + X$  reaction can be reconstructed from the measured 4-vectors of the photon and one of the detected nucleons ie.  $M_{X_i}^2 = (E_\gamma + m_{N_i} - E_{N_i})^2$

-  $(\mathbf{p}_\gamma - \mathbf{p}_{N_i})^2$  for  $i=1,2,3$ . For on-shell pion production  $(M_{X_i}/m_\pi)^2$  should be  $\sim 1$  for the nucleon involved.

Fig. 2 shows a comparison of the predicted  $(M_X/m_\pi)^2$  distributions with the experiment. Both the model and experiment have been restricted to  $E_m^{3B} \leq 100$  MeV to include all the strength from the direct  $3N$  process but reduce the contributions from processes involving FSI. The distributions of  $(M_X/M_\pi)^2$  are presented for two of the three detected nucleons, the neutron and the more forward proton (the backward proton is much less likely to arise from an initial  $N\pi$  process due to kinematic restrictions). The experimental data for both the proton and neutron exhibit a peak around  $m_\pi$  with a tail of strength extending to negative  $(M_X/M_\pi)^2$  values.

The VM simulations of these distributions are shown in the 2D scatter plot and in the projections. The tendency of the  $N\pi + ABS$  contribution to cluster near to  $(M_X/M_\pi)^2 = 1$  is clearly visible. The  $3N$  and  $2N + FSI$  mechanisms are predicted to give some strength in this region but with relatively more strength in the negative tail. The relative strength in the peak and tail regions of the experimental data cannot be well described by the VM without the reduction in the relative strength of the  $N\pi + ABS$  process.

A further indication of the contributions from different reaction mechanisms can be obtained from the photon energy dependence of the cross section which is shown at the top of Fig. 3 for  $E_m^{3B} \leq 50$  MeV,  $E_m^{3B} \leq 100$  MeV and  $E_m^{3B} \geq 100$  MeV. The  $E_m^{3B} \leq 50$  MeV cut restricts the excitation of the residual nucleus to that expected following the knockout of three ( $1p$ ) shell nucleons, whilst the  $E_m^{3B} \leq 100$  MeV cut includes knockout from all shell combinations and includes most of the  $3N$  strength predicted by the VM (see Fig. 1). After the reduction of the  $N\pi + ABS$  strength the VM gives a good description of the experimental data for  $E_m^{3B} \leq 100$  MeV and accounts for the observed strong resonance structure in the  $\Delta$  region. Good agreement is also observed with the  $E_m^{3B} \geq 100$  MeV data for photon energies below  $\sim 450$  MeV. For higher photon energies the observed excess strength compared to the VM prediction may be attributed to  $2\pi$  production pro-

cesses which contribute at these energies and are not included in the model.

As an indication of the success to be expected in removing the contributions of processes other than  $3N$  from the data, the lower part of Fig. 3 presents the photon energy dependence of the cross section after applying the restriction  $(M_X/M_\pi)^2 \leq -1.5$  to the neutron and more forward proton and thus rejecting the major part of the  $N\pi + ABS$  strength for  $E_m^{3B} \leq 100$  MeV (see Fig. 2). The predicted cross sections in this low missing energy region now show little sensitivity to the initial strength of the  $N\pi + ABS$  process and are in fair agreement with the data in both shape and magnitude. The agreement for  $E_\gamma$  below  $\sim 250$  MeV, where  $2N + FSI$  alone is predicted to contribute, gives confidence in the description of this process by the model.

With the above kinematic conditions almost half the cross section for photon energies around 400 MeV is predicted to arise from the absorption of the photon by three interacting nucleons. Only one other mechanism,  $2N$  knockout which is well understood, now competes with the  $3N$  mechanism at low missing energies, which produces a very favourable situation for extracting information on the strength and  $E_\gamma$  dependence of the  $3N$  component. The different  $E_\gamma$  dependence predicted for the  $3N$  and  $2N + FSI$  processes is also beneficial in this regard. Measurements for lighter nuclei to reduce FSI and with wider acceptance detectors and good statistical accuracy would be especially valuable for isolating the contribution of direct  $3N$  absorption and studying the mechanisms responsible.

## REFERENCES

1. J.L. Friar, D. Hüber, U. van Kolck, Phys. Rev. C 59 (1999) 53.
2. W. Glöckle *et. al.*, Nucl. Phys. A 684 (2001) 184c.
3. S.C. Pieper, V.R. Pandharipande, R.B. Wiringa, and J. Carlson, Phys. Rev. C 64 (2001) 014001.
4. J.L. Friar *et. al.*, Phys. Lett. B 311 (1993) 4.
5. J. Carlson, Phys. Rev. C 38 (1998) 1879.; A. Nogga, H. Kamada, W. Glöckle, and B. R.

- Barrett, Phys. Rev. C 55 (2002) 054003.
6. E. Epelbaum *et al.*, arXiv:nucl-th/0201064
  7. A. Lehmann *et al.*, Phys. Rev. C 55 (1997) 2931.
  8. A. Lehmann *et al.*, Phys. Rev. C 56 (1997) 1872.
  9. B. Kotlinski *et al.*, Eur. Phys. J. A 1 (1998) 435.
  10. G. Audit *et al.*, Nucl. Phys. A 614 (1997) 461; Phys. Lett. B 312 (1993) 57; Phys. Rev. C 44 (1991) R575; A. J. Sarty *et al.*, Phys. Rev. C 47 (1993) 459.
  11. P.D. Harty *et al.*, Phys. Rev. C 57 (1998) 123.
  12. D.P. Watts *et al.*, Phys. Rev. C 62 (2000) 014616.
  13. R.C. Carrasco and E. Oset, Nucl. Phys. A 536 (1992) 445; *ibid* A 570 (1994) 701.
  14. R.C. Carrasco, E. Oset, and L.L. Salcedo, Nucl. Phys. A 541 (1992) 585.
  15. M.J. Vicente-Vacas and E. Oset, Nucl. Phys. A 568 (1994) 855.
  16. T. Lamparter *et al.*, Z. Phys. A 355 (1996) 1.
  17. G.E. Cross *et al.*, Nucl. Phys. A 593 (1995) 463.
  18. S.J Hall *et al.*, Nucl. Inst. and Meth. A 368 (1996) 698; I. Anthony *et al.*, *ibid* A 301 (1991) 230.
  19. I.J.D. MacGregor *et al.*, Nucl. Inst. and Meth. A 382 (1996) 479.
  20. P. Grabmayr *et al.*, Nucl. Inst. and Meth. A 402 (1998) 85.
  21. J. C. McGeorge (private communication); D. Branford *et al.*, Phys. Rev. C 61 (1999) 014603.
  22. D.A. Jenkins, P.T. Debevec, and P.D. Harty, Phys. Rev. C 50 (1994) 74.
  23. I.J.D. MacGregor *et al.*, Phys. Rev. Lett. 80 (1998) 245.

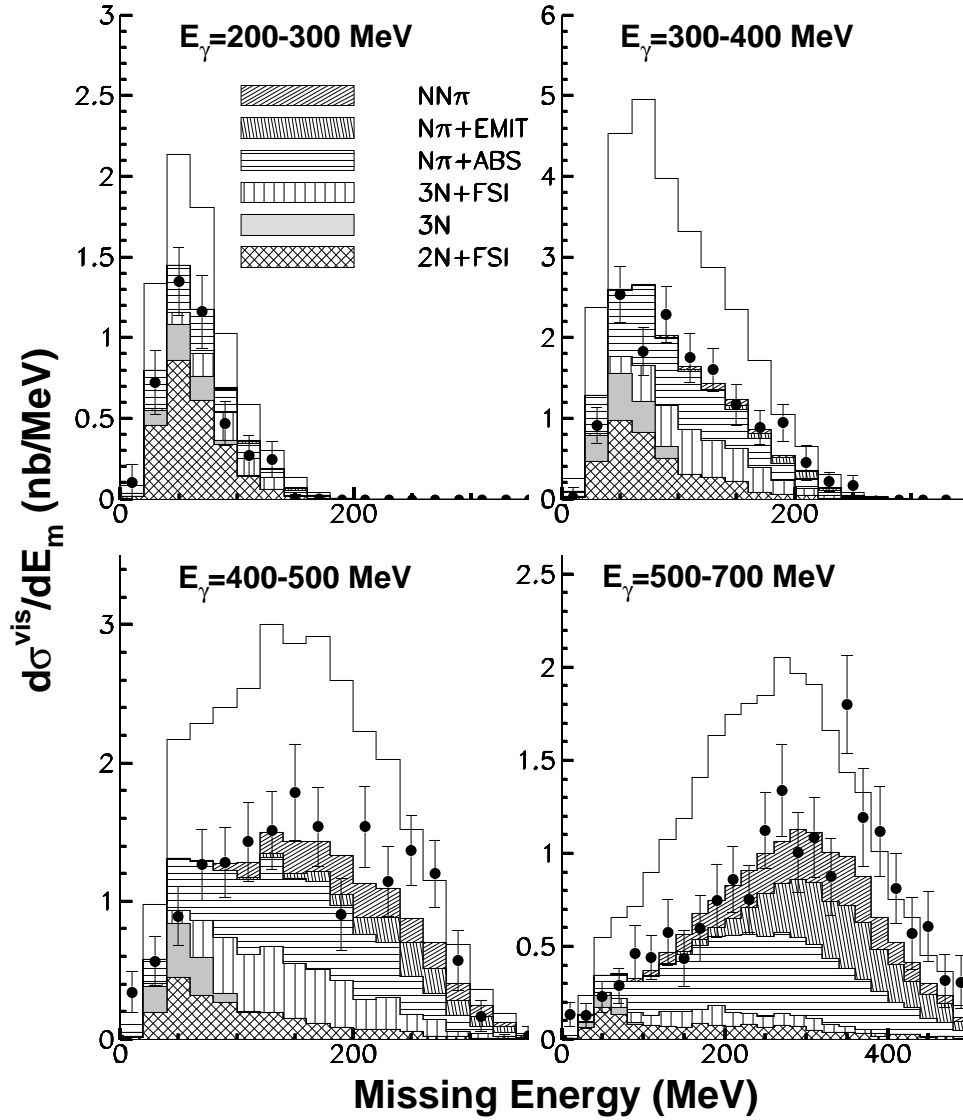


Figure 1. Three-body missing energy distributions for the  $^{12}\text{C}(\gamma, ppn)$  reaction. The shaded histograms show the VM predictions for the different mechanisms indicated by the key on the figure. The solid line shows the total cross section without the reduction of the  $N\pi + \text{ABS}$  prediction (see text).

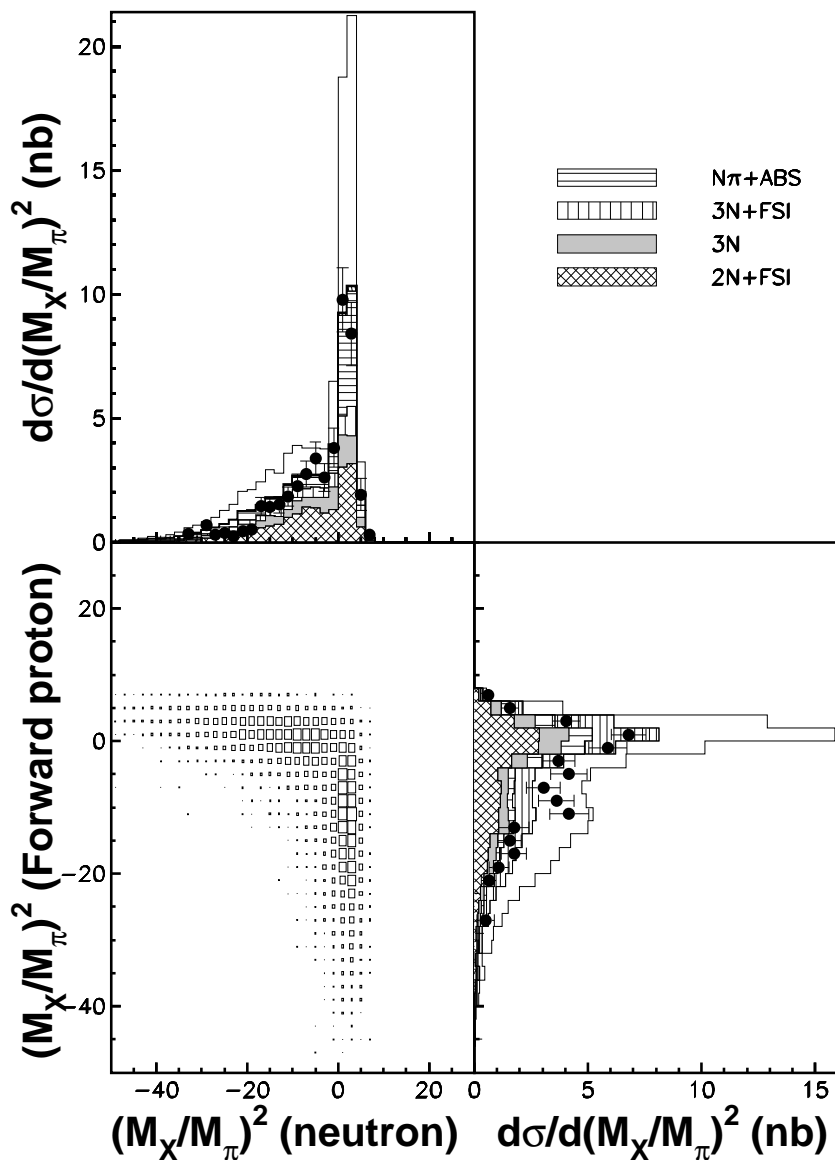


Figure 2. Measured and predicted  $(M_X/M_\pi)^2$  distributions for the  $^{12}\text{C}(\gamma, ppn)$  reaction at  $E_m^{3B} \leq 100$  MeV and  $E_\gamma = 150\text{-}500$  MeV. Bottom left panel shows the Valencia model predictions of  $(M_X/M_\pi)^2$  for the neutron versus the forward proton. The projections onto the x and y axes (shaded histograms) are compared with the experimental data in the top left and bottom right panels. The solid line shows the total cross section without the reduction of the  $N\pi + ABS$  prediction (see text).

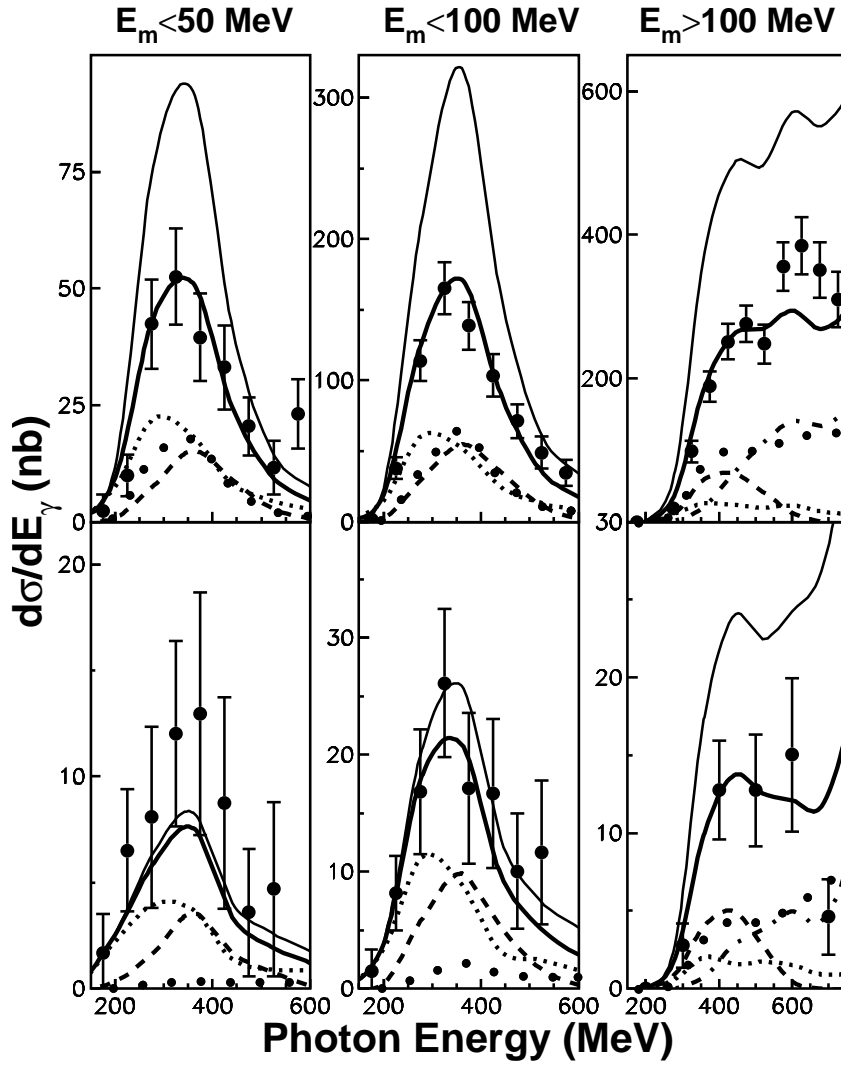


Figure 3. The  $^{12}\text{C}(\gamma, ppn)$  cross section as a function of photon energy presented for three  $E_m^{3B}$  regions indicated in the figure. The lower figures have the additional cut  $(M_X/M_\pi)^2 \leq -1.5$  for the neutron and most forward-angle proton. The total prediction of the (modified) Valencia model is shown by the thick solid line and the separate contributions from the  $2N + FSI$ ,  $3N$  (with or without FSI),  $N\pi + ABS$  and  $NN\pi/N\pi + EMIT$  process are shown by the short dash, long dash, dotted and dot-dashed lines respectively. The thin solid line shows the total VM without reducing the  $N\pi + ABS$  strength (see text).